ResearchGate

See discussions, stats, and author profiles for this publication at: https://www.researchgate.net/publication/351242168

Regulated color-changing metallic glasses

Article *in* Journal of Alloys and Compounds · April 2021

DOI: 10.1016/j.jallcom.2021.160139

CITATIONS
0

READS
39

10 authors, including:

Peng-Fei Wang
Chinese Academy of Sciences
2 PUBLICATIONS **0** CITATIONS
SEE PROFILE

Ming Liu
Chinese Academy of Sciences
11 PUBLICATIONS **42** CITATIONS
SEE PROFILE

Jiri Orava
Jan Evangelista Purkyně University
101 PUBLICATIONS **1,575** CITATIONS
SEE PROFILE

Yonghao Sun
Institute of physics china
27 PUBLICATIONS **626** CITATIONS
SEE PROFILE

Some of the authors of this publication are also working on these related projects:

glass ceramics; View project

ultrastable glass, enhanced surface mobility View project

All content following this page was uploaded by Peng-Fei Wang on 07 May 2021.

The user has requested enhancement of the downloaded file.

Journal of Alloys and Compounds 876 (2021) 160139

Contents lists available at ScienceDirect

Journal of Alloys and Compounds

journal homepage: www.elsevier.com/locate/jalcom

Regulated color-changing metallic glasses

P.F. Wang[a,b], H.Y. Jiang[a,b], J.A. Shi[b], M. Liu[c], L. Gu[a,b], W. Zhou[b], J. Orava[d,e], Y.H. Sun[a,b,g,*], W.H. Wang[a,b,c,g], H.Y. Bai[a,c,f,g,*]

[a] Institute of Physics, Chinese Academy of Sciences, 100190 Beijing, China
[b] School of Physical Sciences, University of Chinese Academy of Sciences, 100049 Beijing, China
[c] Qian Xuesen Laboratory of Space Technology, 100094, Beijing, China
[d] Faculty of Environment, Jan Evangelista Purkyne University in Usti nad Labem, Pasteurova 3632/15, Usti nad Labem 400 96, Czech Republic
[e] IFW Dresden, Institute for Complex Materials, Helmholtzstr. 20, 01069 Dresden, Germany
[f] Center of Materials Science and Optoelectronics Engineering, University of Chinese Academy of Sciences, 100049 Beijing, China
[g] Songshan Lake Materials Lab, 523808 Dongguan, Guangdong, China

ARTICLE INFO

Article history:
Received 3 February 2021
Received in revised form 19 April 2021
Accepted 22 April 2021
Available online 30 April 2021

Keywords:
Metallic glass
Oxidation
Surface
Amorphous oxides
Color changing

ABSTRACT

A new type of color-changing metallic glasses is discovered: the color can change continuously and spontaneously under ambient conditions. The colors are created mostly by the light interference in the surface metallic-oxide layer and partially by the optical bandgap energy of the formed yttrium-doped cerium oxide. Although metal oxidation is a natural consequence for most metals, this series of yttrium-doped and cerium-based metallic glasses are special because i) the oxidation is continuous, allowing color-changing; ii) the oxide layer is uniform in thickness avoiding stain and corrosion; and iii) the colors can change as fast as in days. The color-changing functionality is greatly connected to the oxygen affinity of the cerium constituent, the glassy structure devoid of grain boundaries, and the regulation from the yttrium dopant. This work not only demonstrates a new direction for metal oxidation but also points out new applications of metallic glass.

© 2021 Elsevier B.V. All rights reserved.

1. Introduction

Colorful materials are a long-lasting desire throughout history. Cloisonné vase [1], the Lycurgus Cup [2] and stained glasses [3] have been admired for centuries because of their representative beauty. Besides, surface colors of commodities can satisfy customers' aesthetic taste; the latest smartphones and laptops have more than five frame colors. Colors in metals are quantum effects. Because the bandgap energy between the 5d and 6s electron orbits of gold is 1.9 eV matching the photon energy of blue light, gold absorbs blue lights and appears yellow. Colors on metals, however, are predominantly created by three mechanisms: i) by tuning the optical bandgap energy of co-alloyed metallic oxides with nitrogen or oxygen doping [4,5]; ii) by plasmonic interactions between light and nanostructures [6,7]; and iii) by light interference generated from an oxidized surface layer of metals [5]. Well-known examples are titanium-based alloys whose surface is colorized by electrochemical oxidation forming transparent oxide of thickness matching the interference conditions [8–11]. These coloring methods are appropriate for forming stable colors but are unsuitable if color-changing is required, i.e., color changes over time due to continuous chemical reactions with the environment. Bronze is a typical color-changing alloy: starting from golden color, bronze gradually turns to green by reacting with oxygen, water and carbon dioxide, and forming basic copper carbonate. While bronze is attractive for its aesthetic taste, its spontaneous colorization is too slow (in decades) to appreciate. Therefore, it is necessary to develop metallic materials that have faster color-changing rate.

To develop such color-changing metals, oxidation at ambient conditions is selected as the reaction type. The oxidation of metals proceeds in three stages. At the initial stage, owing to tunneling and thermal emission, electrons quickly migrate from a metal/oxide interface to an oxide/air surface and form different types of anions (O_2^{2-}, O_2^-, O^-) with the oxygen species. An electric potential (Mott potential) [12–14], set by positive metal ions at a metal/oxide interface and the negative oxygen ions at an oxide/air surface, quickly saturates. Then, the Mott potential and chemical potentials ($\mu_{[M]^+}$ at a metal/oxide interface; $\mu_{[O]^-}$ at an oxide/air surface) both assist the migration of metal cations and oxygen anions enhancing the oxide

* Corresponding authors at: Institute of Physics, Chinese Academy of Sciences, 100190 Beijing, China.
E-mail addresses: ysun58@iphy.ac.cn (Y.H. Sun), hybai@iphy.ac.cn (H.Y. Bai).

https://doi.org/10.1016/j.jallcom.2021.160139
0925-8388/© 2021 Elsevier B.V. All rights reserved.

growth [14,15]. Next, electron tunneling and ionic diffusion are inhibited with thickening of a surface oxide layer due to the attenuation of Mott potential [16]. While the overall oxidation is slowed down, local Mott and chemical potential may keep promoting the local oxidation. Eventually, oxidation is ceased except for thermal-emission-induced slow oxidation. The above-mentioned procedures are finished when an oxide layer becomes compact; otherwise, the steps will continuously be repeated [17].

Applications of color-changing metals having spontaneous surface colorization under ambient conditions require the oxide layer growth to be i) continuous and ii) uniform in thickness to avoid stained surfaces. Continuous oxidation depends on temperature. For example, the chromium oxide layer in stainless steels is compact at room temperature but not at temperatures above 1000 K [18]. Cerium has an incompact surface layer at room temperature making its room-temperature oxidation continuous [19]. The compactness of the oxide layer predominantly depends on a *Pilling-Bedworth* ratio (PBR – defined as a ratio of a consumed oxide to metal to the specific volume). When PBR is low, the density of an oxide matches that of base metal and then the oxide-layer growth stops after the initial stage of oxidation. For example, aluminum oxide is stable because of its low PBR of 1.28 (Ref. [19,20]). When PBR is high, a density mismatch exists, microcracks are formed in the oxide layer generating local fast-diffusion pathways for cations and anions [21]. A uniform growth of the oxide layer requires no grain boundaries. For polycrystalline metals, the oxidation rate at the grain boundary is several orders of magnitude higher than that on the lattice [15,22]. Lacking grain boundaries, metallic glasses (MGs) have more homogeneous surface structure without preferential templating sites for oxidation, and hence an oxide layer of naturally-defined uniform thickness can be grown.

Although the oxidation and optical properties of MGs have been studied in many cases [23–27], their potential as color-changing metals has never been explored. Besides, rare-earth elements like cerium are frequently used in pigments [28] and optical materials [29,30]. Therefore, a combination of the optically-active rare-earth oxides and the mechanical performance of MGs [31,32] is expected to bring color-changing metals.

2. Methods

$(Ce_{0.69}Al_{0.10}Cu_{0.20}Co_{0.01})_{100-x}Y_x$ (x = 0, 1, 3, 5, 10, 15, 20 at.%) MGs were selected in the present work. For simplicity, S0, S1, S3, S5, S10, S15, and S20 are used to represent the $(Ce_{0.69}Al_{0.10}Cu_{0.20}Co_{0.01})_{100-x}Y_x$ MGs where S denotes sample, and the number after S denotes x. The alloys were prepared by arc-melting the high purity Ce (99.5%), Al (99.9%), Cu (99.9%), Co (99.9%) and Y (99.5%) elements into ingots, and then re-melted for five times to ensure compositional homogeneity under Ti-gettered argon atmosphere. The glassy ribbons, about 50 μm thick and 2 mm wide, were obtained by melt-spinning the molten master ingot onto a copper wheel under argon atmosphere. The amorphicity was confirmed by X-ray diffraction (Bruker D8) and by selected area electron diffraction (SAED, JEOL 2100 Plus). Thermal properties were measured by a differential scanning calorimeter (DSC, Perkin Elmer DSC 8000) at a heating rate of 20 K min^{-1}. The glass-transition temperature (T_g) ranges from 350 K to 360 K for all MG ribbons. Ribbons' surface was imaged under an optical microscope (Leica DM 2700 M), and the ribbons' cross-section was examined in a high-resolution transmission electron microscopy (HRTEM, JEOL 2100 Plus). Reflectance spectra were measured by a fiber-optic spectrometer (Light Source: EQ99, Energetiq; spectrometer: HR 2000, Ocean Optics) in the spectral range of 350–800 nm. Diffuse reflectance spectra were measured by a universal measurement spectrophotometer (Cary 7000, Agilent). The oxide layer thickness was measured by a dual-beam electron microscope (Thermo Fisher Helios G4 CX) or by transmission electron microscope (TEM, JEOL 2100 Plus). The mechanical properties of the oxide layer were measured by a nano-indentation system (Bruker Hysitron TI 950). Oxidation kinetics were measured by a thermal gravimetric analyzer (TGA, Mettler Toledo TGA2). Sample displays were obtained by picosecond-pulsed laser cutting at a laser wavelength of 355 nm and an output power of 20 W (Photonics Industries International Inc.). The colors were quantitatively evaluated by calculating the chromaticity x and y using the CIE color space standardized by the international commission on illumination ($x = X \div (X+Y+Z)$, $y = Y \div (X+Y+Z)$, and $z = 1-x-y$). The X, Y and Z were measured using a colorimeter (NR110, 3nh with D65 illuminant and using at an aperture size of 4 mm). Fluorescent microscope images were taken under fluorescence microscope (BX51, Olympus). The photoluminescence spectrum of the samples was quantified by a confocal micro-photoluminescence system (IK5551R-F, Kimmon Koha Co. Ltd.) at an emission wavelength of 325 nm.

3. Results and discussion

3.1. The colors of metallic glasses and photoluminescence

Natural colors appear on the surface of the Y-doped and Ce-based MG ribbons after aging at ambient conditions. The decorations and ribbons of a series of Y-doped Ce-based MGs are attached to a cylindrical black support, and the overall is imaged with a camera. Fig. 1a shows the general look of a series of the 400-day aged S1, S5, S10, S15, S20 ribbons, and the laser-cut apple-, dolphin- and star-shaped decorations of the 43-day or 13-day aged S5 ribbons. Clearly, blue color is shown on the surface of the 43-day aged S5 decorations, and in contrast, yellowish color is shown on the surface of the 13-day aged S5 decorations. On the other hand, even after 400-day aging in air and at room temperature, all Y-doped Ce-based MG ribbons show bright but different colors with high quality, e.g., magenta color on the surface of S1 ribbon and green color on the surface of S15 ribbon. In more details, the colors on the two ends of MG ribbon are slightly different, indicating that the colors may change with the relative angles of the incident light at the surface (these ribbons are attached to the cylindrical support). Strong reflection is clearly shown in the middle of the ribbon, e.g., S10 ribbon.

Apart from the natural colors, photoluminescence is found on these MG ribbons, too. Fig. 1b exhibits the fluorescent microscope images of the 410-day aged S5 ribbon, where the colors on the MG ribbons are different without and with a violet light source. Photoluminescence spectra are provided in the Fig. S1 under a ultraviolet

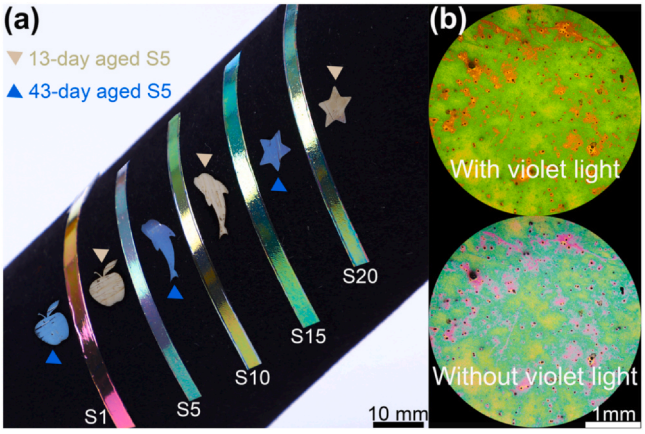

Fig. 1. (a) General look of a series of the 400-day aged Y-doped and Ce-based MG ribbons (S1, S5, S10, S15 and S20). The laser-cut decorations (in dolphin, apple or star shapes) are the 43-day and the 13-day aged S5s. (b) Fluorescent microscope images of the 410-day aged S5 MG ribbon with and without violet source excitation.

source of $\lambda = 325$ nm. Peaks representing the orange color ($\lambda = 610$ nm) and green color ($\lambda = 535$ nm) have the largest intensities correlating well to the fluorescent microscope images of the 410-day aged S5. Similar peak positions are found in the photoluminescence spectra of another 46-day aged S1.

3.2. The color-changing functionality of the Y-doped and Ce-based MGs

The studied MG ribbons contain active elements, e.g., Ce and Y, and inevitably oxidize in air and at room temperature. With surface oxide layer thicken, colors will be created when the layer thickness matches the interference conditions in the visible light frequency range. Then, the Ce-based MGs are spontaneously colorized at ambient conditions during aging. Color appearance with high-quality is attributed to the unique disordered microstructure of Ce-based MGs, lacking grain-boundary. Different colors are shown on the surface of a series of the 400-day aged MG ribbons (Fig. 1a), which implys the significant effect of yttrium doping on the surface colors regulation. Moreover, the bright color is attributed to the "glaze" surface of the as-spun ribbon acting as a mirror: the surface roughness of the high-quality as-spun Ce-based MGs can be as low as ± 1 nm [33], and hence no polishing is required to ensure low roughness. The optical reflectance in the range of the visible light is 70%. In other words, the Y-doped Ce-based MGs has the functionality of color-changing. Therefore, the Ce-based MGs gain an immediate aesthetic value through spontaneous colorization.

Fig. 2a and b show the surface colors of the S0 and S5 ribbons after aging at ambient conditions for 1–117 days. Colors on the surface of S0 ribbons (Fig. 2a) change from yellow to violet. In contrast, colors on the surface of S5 MG ribbons change from yellowish to violet to green and to violet again (Fig. 2b). In more details, with the addition of 5 at% of Y into $Ce_{69}Al_{10}Cu_{20}Co_1$ MG ribbons, more colors appear, and the changes of color are faster. Furthermore, the color gets deeper with time. The corresponding wavelengths of the colors are evaluated by a three-primary colors (RGB) standard (Fig. 2c) [34]. For S0, only one cycle of color toning is detected in 100 days; for S5, 2.5 cycles of color toning are obtained in 100 days.

The spontaneous colorization is a dynamic process (Fig. 2c). The color exhibits a repeating sequence in tone and changes from warm to cold tones first and then repeats. The continuous changing of the surface color overtime is attributed to the continuous surface oxide growth. The surface oxide layer thicken with time is carefully verified by SEM in S0 and S5 ribbons after aging for various days (Fig. S2). At the same aging time, the oxidation layer of S5 ribbon is always thicker than that of the S0 ribbon indicating that the additional Y of 5 at.% speeds up the oxidation. Even though the color-changing of the surface of Ce-based MGs is as fast as in days, the ability of continuous color-changing of the surface with high quality can be maintained. With the knowledge of colors and color-changing rates at the corresponding Y addition, the Ce-based MG colorization is thus regulated.

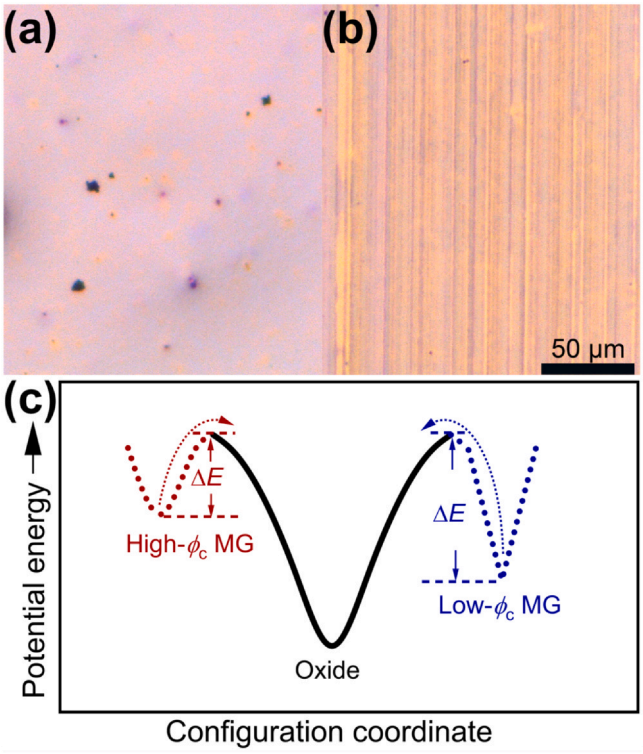

Fig. 3. Image captured from (a) the free surface and (b) the wheel side of the 6-day aged S5 ribbon. (c) A schematic energy-landscape diagram of MG oxidation. Cooling rate (ϕ_c) controls the energy state of the MGs and hence affects the activation energy of oxidation (ΔE).

3.3. Effects of the cooling rate on spontaneous colorization

Colors appearing on the free surface and wheel side of the MG ribbons are different after 6-day aging in air and at room temperature (Fig. 3a and b). Besides, the color-changing rate of the 1 mm-thick bulk MG plates is much slower than that of the MG thin ribbons of the same composition. Melt-spun ribbons are made by injecting the molten liquid onto a spinning copper wheel, and hence

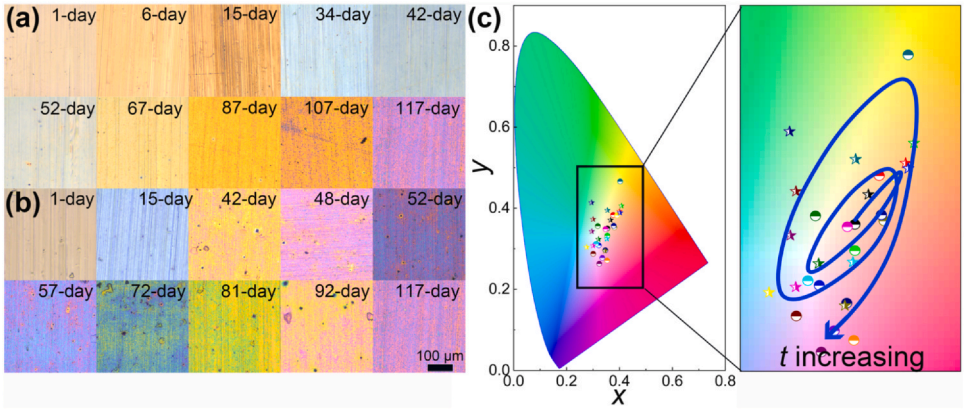

Fig. 2. Surface colors of (a) S0 and (b) S5 ribbons after aging at ambient conditions for 1–117 days. (c) The chromaticity diagram of the colorized S5 ribbons. The colors were measured either by a colorimeter (stars) or read from a picture in Adobe Photoshop software (circles). Inset is an enlarged view of the colorized region where the curved arrow represents increasing time.

the side of the ribbon which comes into the contact with the copper wheel (wheel side) has a higher cooling rate (ϕ_c) and exhibits more of *Plateau–Rayleigh* instability-like features (Fig. 3b) than the side exposed to argon atmosphere (free surface) [35]. These *Plateau–Rayleigh* instability-like features are common in other MG melt-spun ribbons, and their widths and spacings are beyond the light-interference conditions, *not* corresponding to the colorization. The bulk MG plates are suction-casted into a copper mold, by which the method is expected to have a ϕ_c order-magnitude lower than melt-spinning. It is then wondered that ϕ_c may play an important role on the spontaneous colorization. As a typical metastable material, MGs obtained with high ϕ_c have high stored energy that helps MGs to overcome the energy barrier of oxidation. As schematically explained in Fig. 3c, MG of high stored energy has shallow energy basin and small energy barrier of oxidation (ΔE), whereas MG of low stored energy has deep energy basin and big ΔE. The decrease of ΔE indicates that more MG surface atoms could be oxidized explaining why a high-ϕ_c MG has a faster oxidation rate than the low-ϕ_c MG. It needs to be pointed out that due to the low T_g of these Ce-based MGs, room temperature is high enough to promote fast relaxation, thereby the energy difference caused by ϕ_c will be eliminated in 10 days [36]. Furthermore, the surface color on the free surface appears deeper (or more saturated) than that on the wheel side, implying that the oxide layer grows more compact on the free surface than on the wheel side due to slower oxidation. Therefore, ϕ_c has a strong effect on the oxidation rate, and on the spontaneous colorization of the MGs.

3.4. Color reemergence and color contrast of a grinded MG

After 42-day aging, yellow color appears on the surface of S5 ribbon (Fig. 4a). Mechanical grinding is then applied to remove the surface oxide, and the ribbon loses its color. However, the S5 ribbon re-gains its yellow color on further aging in 33 days after grinding demonstrating that the oxidized layer is self-healable (Fig. 4b). Since the yellow color is reemerged in 33 days instead of 42 days, it suggests that the oxidation rate is increased after grinding. This may be attributed to the rougher surface left after grinding, which acts as the heterogeneous site for nucleating oxide and promoting faster oxidation.

After grinding, some scratches and dots are left on the surface generating a color contrast between them and the overall surface (Fig. 4b). Color contrasts can also be found on other S5 ribbons with surface flaws induced either at the manufacturing or processing stages. Surface flaws give heterogeneous sites that assist in enhancing the local color-changing rate. Unlike the uniform colors on the smooth surfaces, the color contrasts created by these surface flaws have their own aesthetic values. Fig. 4c presents a yellow surface embellished with some blue cavities appearing similar aesthetic features of corals, and Fig. 4d exhibits a golden scratch on a purple surface mimicking a flash of lightning during the night. The variable oxidation rates between the surface and the flaws open up the possibilities for designing the aesthetic appearance of MGs via manmade surface flaws. Therefore, from an aesthetic point of view, the surface of the color-changing metals could be "painted" through manmade flaws.

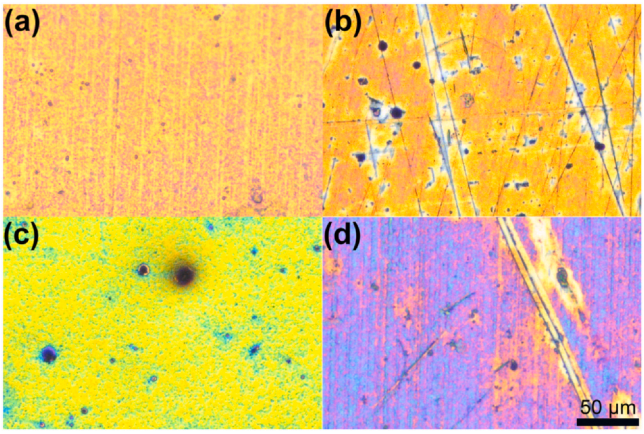

Fig. 4. (a) Yellow appears on the 42-day aged S5 ribbon. (b) Yellow reemerges in 33-day after mechanical polishing the sample of part (a). (c) Casted cavities are found on the surface of the 81-day aged S5 ribbon, and (d) as-spun scratches are left on another 57-day aged S5 ribbon.

3.5. The angular reflectance spectra

Fig. 5a shows the reflectance spectra of the 111-day aged S5 ribbon where the spectra of light source (dashed line) is also shown for a comparison. Here, the incident angle (θ) is defined as the angle from the surface, *not* from the normal. The position of the reflectance maximum (λ_1) measured at θ of 70° is 604 nm, consistent with the color captured under an optical microscope at $\theta = 90°$. As shown in Fig. 5a, when θ shifts to smaller angles (50°, 30°, 10°), λ_1 decreases (596 nm, 558 nm, 551 nm). Meanwhile, when testing another 76-day aged S5 at $\theta = 60°$ (Fig. 5b), the position of λ_1 is 510 nm. In comparison with λ_1 of the 111-day aged, there is an obvious increase of λ_1 with the increasing t.

Both the increase of λ_1 with increasing θ and the red shift of λ_1 with increasing t indicate the continuous thickening of the surface oxide layer (Fig. 5). For the 111-day aged S5, the thickness of the oxide layer (d) is estimated to be 221 ± 29 nm ($d = \lambda_1/(2n_2\sin\theta)$; n_2 – the refractive index of the oxide of 1.57 ± 0.02 as measured) and d is about 187 nm for the 76-day aged S5, consistent with the thickness measured by SEM (Fig. S2). In other words, the continuous surface oxide growth is the reason why the surface color continues to change. On the other hand, valleys shown in Fig. 5a demonstrate the existence of intrinsic colors. Measured by the diffuse reflectance spectra, the electron bandgap energies of the surface oxides detected on the 155-day aged S0 and S5 ribbons are 2.42 eV and 2.99 eV, respectively, corresponding to the absorption of green and purple colors (Fig. S3) [5,37,38]. We attribute the origin of this intrinsic color to the electron bandgap energy of the Y-doped CeO_2 because cerium oxides are attractive as pigments due to their yellow coloration [28], and their colors can be easily changed by dopants [39].

3.6. The SEM and HRTEM analyses

Fig. 6a shows the SEM examination on the wheel-side surface of the 79-day aged S5, and striped texture is present on the surface. A cross section of the surface oxide layer is exposed by ion etching, and from SEM, distinguishing contrast presents the uniform surface oxide layer with the thickness about 269 nm for the 114-day aged S5 (Fig. 6b). For more detailed information, the surface oxide layer of the 46-day aged S5 is further investigated by HRTEM (Fig. 6c). Three distinct regions are identified: oxide, affected region and the MG substrate, where the thickness of the oxide layer about 160 nm for the 46-day aged MG. Here, distinct dark-and-bright contrast appears in the oxide layer correlating with some intrinsic body structures. The formed oxide is amorphous, as confirmed by SAED (insets of Fig. 6d and e).

Undifferentiated contrast on the surface suggests that the oxidation rate on every surface location is nearly the same (Fig. 6a). As a result, the thickness of the surface oxide layer appears uniform. However, distinct dark-and-bright contrast appears in the oxide layer (Fig. 6c), suggesting a heterogeneous structure of the thin layer. According to the *Lambert-Beer* law, the intensity is attenuated by both oxide thickness and density. Since the oxide thickness is uniform, the contrast is attributed to the varying oxide density.

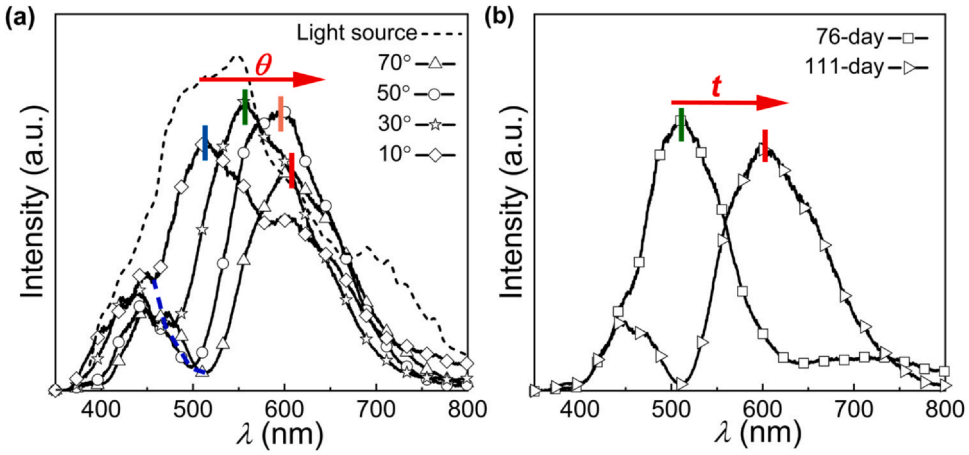

Fig. 5. Reflectance spectra of the 111-day and 76-day aged S5 ribbons. (a) Angular (θ) dependence of the reflectance for the 111-day aged S5. (b) Time (t) dependence of the 76-day and 111-day aged S5 measured at $\theta = 60°$.

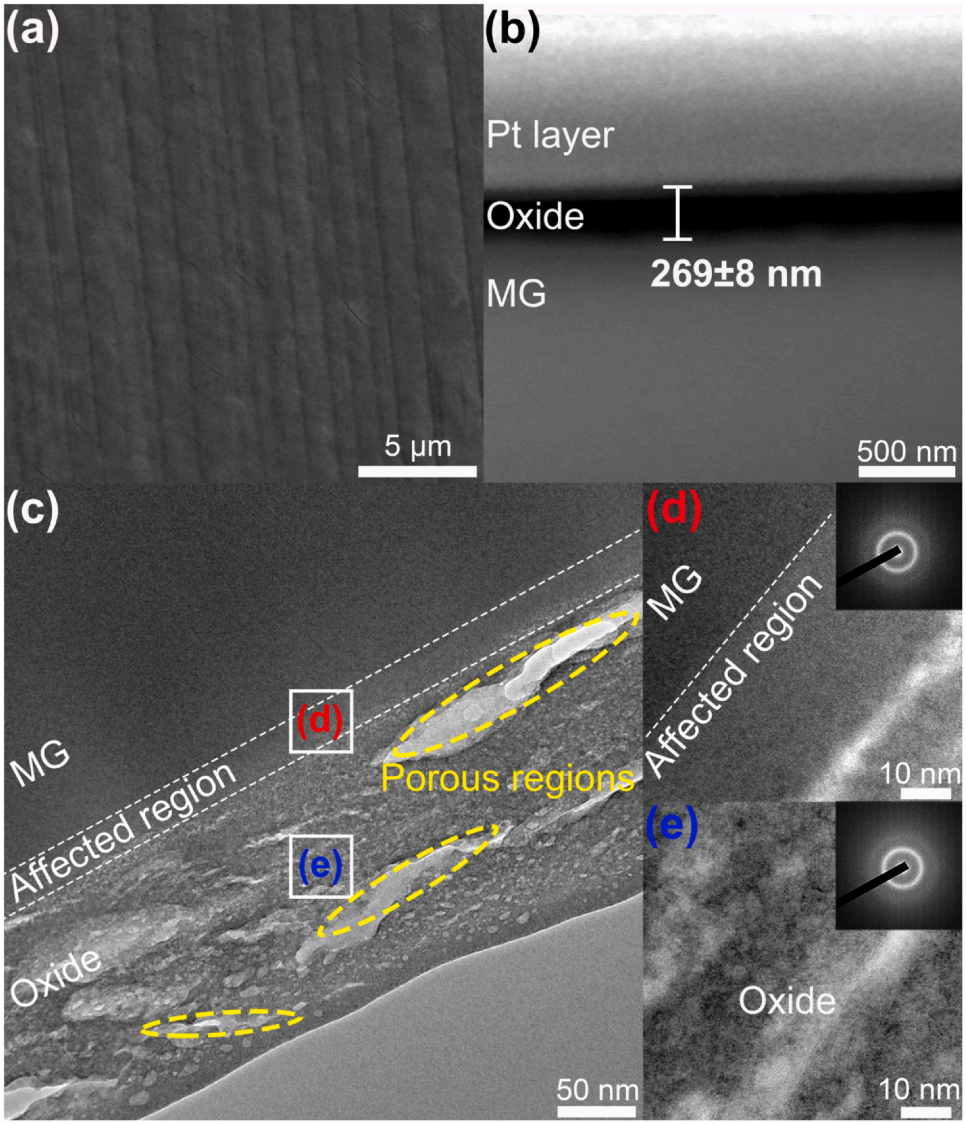

Fig. 6. (a) SEM examination of the wheel-side surface of the 79-day aged S5. (b) SEM image of the cross-section of the 114-day aged S5 ribbon reveals an oxide layer thickness of 269 ± 8 nm. A Pt layer is deposited onto the sample before ion etching to protect the oxide layer and to reduce charging. (c) HRTEM image of the 46-day aged S5 where porous regions are circled in yellow for guidance. A close-up view (d) reveals a 10 nm affected region between the glass and the oxide; and (e) shows a porous oxide layer. SAED patterns (insets) confirm the amorphicity at (d) and (e) locations.

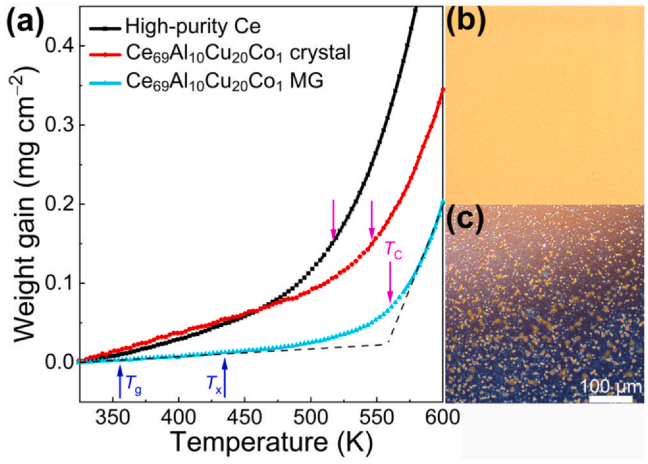

Fig. 7. (a) The weight-gain curves of high-purity Ce, crystalline $Ce_{69}Al_{10}Cu_{20}Co_1$ and S0 on heating at a rate of 10 K min^{-1} under an air-flow of 50 ml min^{-1}. The corresponding temperatures mark the glass-transition temperature (T_g), the end of primary crystallization (T_x) of the glass, and the transition point from slow to fast oxidation (T_c). Optical images of (b) the S0 ribbon after 14-day aging, and (c) of the crystalline $Ce_{69}Al_{10}Cu_{20}Co_1$ ribbon after 5-day aging; both aged at ambient conditions.

Porous regions are then identified. Such structure is pronounced for short-term aging, suggesting a fast dynamics of the oxide growth at the beginning of spontaneous colorization. Yet, the contrast disappears for samples after long-time aging, implying that a compact surface layer has formed. This explains why light color is observed at the beginning whereas deep color is detected after aging. Therefore, the surface-color appearance is not only controlled by the oxide thickness but also by its compactness.

3.7. Thermal gravity analysis

The oxidation kinetics of high-purity Ce, crystalline $Ce_{69}Al_{10}Cu_{20}Co_1$ and S0 are compared (Fig. 7a). A critical temperature T_c, defined by the intersections of the extensions of slow and fast weight gains as shown in Fig. 7a, marks the transition point from low-T (slow) to high-T (fast) oxidation. Below T_c, the oxidation rate of both high Ce and the crystalline counterpart is comparable, and is four times faster than S0 ribbon (Fig. 7a). Above T_c, the oxidation rate of both MG and the crystalline counterpart is comparable, and is lower than high-purity Ce. Compared with the high-purity Ce and the crystalline counterparts, MG has the highest T_c and the lowest weight-gain at T_c. Uniform yellow color is shown on the surface of the S0 ribbon after 14-day aging at ambient conditions (Fig. 7b). In sharp contrast, the surface of the crystalline $Ce_{69}Al_{10}Cu_{20}Co_1$ metal tarnishes after 5-day aging at ambient conditions (Fig. 7c).

Below T_c, the oxidation rate of crystalline counterparts is four times faster than the Ce-based MG ribbon (Fig. 7a) due to the grain boundaries, thus the surface of the crystalline metal tarnishes due to the fast oxidation rate (Fig. 7b and c). Moreover, above T_c, the oxidation rate of Ce-based MG and crystalline counterpart is comparable because T_c is high enough to make Ce-based MG completely crystallized. The highest T_c and the lowest weight-gain at T_c demonstrate good stability of slow oxidation.

4. Discussions

The spontaneous colorization of the Y-doped and Ce-based MGs gains an immediate esthetic taste for color applications. The smooth surface of the melt-spun ribbon provides uniform colors, while designed surface patterns may provide color contrasts. For single-color applications, air isolation, e.g., pasting a plastic tape on the ribbon, can slow down the color-changing rate and maintains the surface colors present at certain days of aging. However, the color-changing functionality itself may create a new phase of applications. How interesting if the frame color of our laptop or cellphone could be spontaneously changed everyday? How surprising if a portrait continuously changes its color contrast? Bronze statue is appealing not only by its golden color when firstly made but also by its green appearance after continuous color changing in ages. For the Y-doped and Ce-based MGs, the waiting time of color changing is greatly reduced.

Finally, we emphasize the benefits of using glassy alloys instead of crystalline alloys for spontaneous surface colorization. The homogeneous structure of MGs, lacking the grain-boundary features, allows for the same oxidation rate on every surface location and for delivering uniform thickness of oxide layers; those are the necessary prerequisites for high-quality color appearance. The melt-spun MG ribbons can have a very smooth surface with a nanometer-scale roughness and hence deliver a glazed surface. With a PBR of 1.50 for the Ce-based MG [19,40], the residual stress is compressive for the oxide and tensile for the MG. Because MGs have an elastic strain-limit as large as 2% (Ref. [41]), nearly 10 times of the crystalline metals, cracking of the surface oxide is less severe for MGs than for their crystalline counterpart. The oxide layer of MG is also more stable against fast oxidation than the crystalline counterpart and the high-purity Ce. In addition, MGs have excellent mechanical performance, including large elastic-strain limit, high strength and for some compositions, a combination of high toughness [31,42,43]. The apparent nano-hardness of the 88-day aged S5 with a 200 nm-thick oxide layer is 2.47 ± 0.06 GPa (the value also accounts for the residual stress in the oxide layer), higher than that of the pristine MG, 2.03 ± 0.02 GPa; the melt-spun ribbons are ductile, for example, the Ce-based MG ribbon can be scissored at room temperature or thermo-plastically moulded in hot water [44,45]. All these characteristics summarized above demonstrate that the Y-doped Ce-based MG ribbons rather than crystalline alloys are good color-changing metals.

5. Conclusions

In summary, a new type of color-changing metals, namely a yttrium-doped cerium-based metallic glass, is developed to be capable of spontaneous colorization at ambient conditions. The achieved colors are regulated, and the formed oxide is self-healable. Colorization appears due to the interfering color from a growing oxide layer on the metallic glass surface and due to the intrinsic color from the optical bandgap energy of the yttrium-doped cerium oxide. The continuous growth of a uniform oxide layer of the cerium-based metallic glass stems from the glass's low T_g, from a low *Pilling-Bedworth* ratio and the glassy structure itself lacking grain boundaries typical in polycrystalline metals. The spontaneous colorization and the unique aesthetic value of the cerium-based color-changing metals open up new directions for both fundamental science and practical applications.

CRediT authorship contribution statement

P.F. Wang: Conceptualization, Methodology, Validation, Formal analysis, Investigation, Writing - original draft, Visualization. **H.Y. Jiang:** Investigation. **J.A. Shi:** Investigation. **M. Liu:** Investigation. **L. Gu:** Resources. **W. Zhou:** Resources. **J. Orava:** Writing - review & editing, Supervision, Funding acquisition. **Y.H. Sun:** Conceptualization, Writing - review & editing, Supervision, Project administration, Funding acquisition. **W.H. Wang:** Resources, Funding acquisition. **H.Y. Bai:** Writing - review & editing, Supervision, Project administration.

Declaration of Competing Interest

The authors declare that they have no known competing financial interests or personal relationships that could have appeared to influence the work reported in this paper.

Acknowledgements

This research was supported by Beijing Municipal Science and Technology Commission [grant number Z191100007219006], the National Key Research and Development Plan [grant number 2018YFA0703603], the Strategic Priority Research Program of the Chinese Academy of Sciences [grant number XDB30000000], the National Natural Science Foundation of China [grant numbers 11790291, 61999102, 61888102, 51971239], and the Natural Science Foundation of Guangdong Province [grant number 2019B030302010]. J.O. acknowledges the assistance provided by the Research Infrastructure NanoEnviCz, which is supported by the Ministry of Education, Youth and Sports of the Czech Republic (LM2018124). J.O. and Y.H.S. acknowledge the financial support of the promising Young scientists award from the Center for International Collaboration (IOPCIC), Institute of Physics, Chinese Academy of Sciences. Prof. Xiulai Xu, Prof. Hong Wei, Shan Xiao, Dr. Fucheng Li, Xiaohong Yan, Yutian Wang and Jiashu Cao from the Institute of Physics, the Chinese Academy of Sciences, Dr. Laiquan Shen, Dr. Mingxing Li, Dr. Haijie Xian and Yuqiang Yan from Songshan Lake Materials Lab, and Cong Tian from Wuhan E-Optics Technology Co. Ltd. are thanked for their help with experiments. Xiaoqing Wu from the University of Science and Technology of China is thanked for stimulating discussion.

Appendix A. Supporting information

Supplementary data associated with this article can be found in the online version at doi:10.1016/j.jallcom.2021.160139.

References

[1] B. Kırmızı, P. Colomban, B. Quette, On–site analysis of Chinese Cloisonné enamels from fifteenth to nineteenth centuries, J. Raman Spectrosc. 41 (2010) 780–790.
[2] F.E. Wagner, S. Haslbeck, L. Stievano, S. Calogero, Q. Pankhurst, K. –P. Martinek, Before striking gold in gold-ruby glass, Nature 407 (2000) 691–692.
[3] S. Capaccioli, G. Ruocco, Relaxation is a two–step process for metallic glasses, Physics 10 (2017) 58.
[4] C. Yang, C. Zhang, L. Liu, Tuning colors in Zr–based thin film metallic glasses, J. Alloy. Compd. 728 (2017) 289–294.
[5] Y. Bu, X.M. Bu, F.C. Lyu, G. Liu, G. Wu, L.L. Pan, L.Z. Cheng, J.C. Ho, J. Lu, Full-color reflective filters in a large area with a wide–band tunable absorber deposited by one–step magnetron sputtering. Adv. Opt. Mater. 8 (2019) 1901626.
[6] A. Kristensen, J.K.W. Yang, S.I. Bozhevolnyi, S. Link, P. Nordlander, N.J. Halas, N.A. Mortensen, Plasmonic colour generation, Nat. Rev. Mater. 2 (2016) 16088.
[7] S.J. Tan, L. Zhang, D. Zhu, X.M. Goh, Y.M. Wang, K. Kumar, C.-W. Qiu, J.K. Yang, Plasmonic color palettes for photorealistic printing with aluminum nanostructures, Nano Lett. 14 (2014) 4023–4029.
[8] I. Sirés, E. Brillas, M.A. Oturan, M.A. Rodrigo, M. Panizza, Electrochemical advanced oxidation processes: today and tomorrow. A review, Environ. Sci. Pollut. Res. 21 (2014) 8336–8367.
[9] V. Zwilling, M. Aucouturier, E. Darque-Ceretti, Anodic oxidation of titanium and TA6V alloy in chromic media. An electrochemical approach, Electrochim. Acta 45 (1999) 921–929.
[10] E. Gaul, Coloring titanium and related metals by electrochemical oxidation, J. Chem. Educ. 70 (1993) 176–178.
[11] M.V. Diamanti, B. Del Curto, M. Pedeferri, Interference colors of thin oxide layers on titanium, Color Res. Appl. 33 (2008) 221–228.
[12] N.F. Mott, A theory of the formation of protective oxide films on metals, Trans. Faraday Soc. 35 (1939) 1175–1177.
[13] N.F. Mott, The theory of the formation of protective oxide films on metals, II, Trans. Faraday Soc. 35 (1940) 472–483.
[14] N.F. Mott, The theory of the formation of protective oxide films on metals.—III, Trans. Faraday Soc. 43 (1947) 429–434.
[15] A. Atkinson, Transport processes during the growth of oxide films at elevated temperature, Rev. Mod. Phys. 57 (1985) 437–470.
[16] A.T. Fromhold, E.L. Cook, Kinetics of oxide film growth on metal crystals: electron tunneling and ionic diffusion, Phys. Rev. 158 (1967) 600–612.
[17] J.L. Leach, Surface oxide films and the breakaway corrosion of uranium, Nature 182 (1958) 1085–1086.
[18] Y. Yamamoto, M.P. Brady, Z.P. Lu, P.J. Maziasz, C.T. Liu, B.A. Pint, K.L. More, H.M. Meyer, E.A. Payzant, A. Creep-resistant, Al_2O_3–forming austenitic stainless steels, Science 316 (2007) 433–436.
[19] W. Haynes, D. Lide, T. Bruno, CRC Handbook of Chemistry and Physics, 97th ed., CRC Press, London, UK, 2017.
[20] E.P. Busso, H.E. Evans, Z.Q. Qian, M.P. Taylor, Effects of breakaway oxidation on local stresses in thermal barrier coatings, Acta Mater. 58 (2010) 1242–1251.
[21] H.E. Evans, H.Y. Li, P. Bowen, A mechanism for stress-aided grain boundary oxidation ahead of cracks, Scr. Mater. 69 (2013) 179–182.
[22] P. Shewrnon, Diffusion in Solids, second ed., Springer, Berlin, 2016.
[23] Z. Xu, Y. Xu, A. Zhang, J. Wang, Z. Wang, Oxidation of amorphous alloys, J. Mater. Sci. Technol. 34 (2018) 1977–2005.
[24] B.S. Yu, Y.H. Sun, H.Y. Bai, W.H. Wang, Highly energetic and flammable metallic glasses, Sci. China Phys. Mech. Astron. 63 (2020) 276112.
[25] J.H. Na, K.H. Han, G.R. Garrett, M.E. Launey, M.D. Demetriou, W.L. Johnson, Designing color in metallic glass, Sci. Rep. 9 (2019) 3269.
[26] J. Liu, Y. Liu, P. Gong, Y. Li, K.M. Moore, E. Scanley, F. Walker, C.C. Broadbridge, J. Schroers, Combinatorial exploration of color in gold-based alloys, Gold Bull. 48 (2015) 111–118.
[27] M.X. Li, S.F. Zhao, Z. Lu, A. Hirata, P. Wen, H.Y. Bai, M.Y. Chen, J. Schroers, Y.H. Liu, W.H. Wang, High–temperature bulk metallic glasses developed by combinatorial methods, Nature 569 (2019) 99–103.
[28] C.E. Castano, W.G. Fahreholtz, M.J. O'Keefe, Cerium oxide (CeO_2), in: G. Koroteenkov, S. Scirè, L. Palmisano (Eds.), Synthesis, Properties and Applications, Elsevier, Netherlands, United Kingdom and United States, 2020(Ch. 6).
[29] R. Si, Y.-W. Zhang, H.-P. Zhou, L.-D. Sun, C.-H. Yan, Controlled-synthesis, self-assembly behavior, and surface-dependent optical properties of high-quality rare-earth oxide nanocrystals, Chem. Mater. 19 (2007) 18–27.
[30] J. Zhou, Q. Liu, W. Feng, Y. Sun, F. Li, Upconversion luminescent materials: advances and applications, Chem. Rev. 115 (2015) 395–465.
[31] C. Suryanarayana, A. Inoue, Bulk Metallic Glasses, second ed., CRC Press, FL, 2017.
[32] C.A. Schuh, T.C. Hufnagel, U. Ramamurty, Mechanical behavior of amorphous alloys, Acta Mater. 55 (2007) 4067–4109.
[33] D. Nečas, P. Klapetek, Gwyddion: an open–source software for SPM data analysis, Cent. Eur. J. Phys. 10 (2012) 181–188.
[34] H.S. Fairman, M.H. Brill, H. Hemmendinger, How the CIE 1931 color-matching functions were derived from Wright–Guild data, Color Res. Appl. 22 (1997) 11–23.
[35] L. Rayleigh, On the instability of a cylinder of viscous liquid under capillary force, Philos. Mag. 34 (1892) 145–154.
[36] T.P. Ge, C. Wang, J. Tan, T. Ma, X.H. Yu, C.Q. Jin, W.H. Wang, H.Y. Bai, Unusual energy state evolution in Ce-based metallic glass under high pressure, J. Appl. Phys. 121 (2017) 205109.
[37] C. Ho, J.C. Yu, T. Kwong, A.C. Mak, S. Lai, Morphology–controllable synthesis of mesoporous CeO_2 nano- and microstructures, Chem. Mater. 17 (2005) 4514–4522.
[38] R. López, R. Gómez, Band–gap energy estimation from diffuse reflectance measurements on sol–gel and commercial TiO_2: a comparative study, J. Sol–Gel Sci. Technol. 61 (2012) 1–7.
[39] C.P. Aby, K.J. Sreeram, B.U. Nair, T. Ramasami, Doped oxides of cerium as inorganic colorants, Color. Technol. 123 (2007) 374–378.
[40] W.H. Wang, The elastic properties, elastic models and elastic perspectives of metallic glasses, Prog. Mater. Sci. 57 (2012) 487–656.
[41] A.L. Greer, Y.H. Sun, Stored energy in metallic glasses due to strains within the elastic limit, Philos. Mag. 96 (2016) 1643–1663.
[42] D.C. Hofmann, J.Y. Suh, A. Wiest, G. Duan, M.L. Lind, M.D. Demetriou, W.L. Johnson, Designing metallic glass matrix composites with high toughness and tensile ductility, Nature 451 (2008) 1085–1089.
[43] M.D. Demetriou, M.E. Launey, G. Garrett, J.P. Schramm, D.C. Hofmann, W.L. Johnson, R.O. Ritchie, A damage-tolerant glass, Nat. Mater. 10 (2011) 123–128.
[44] B. Zhang, R.J. Wang, D.Q. Zhao, M.X. Pan, W.H. Wang, Superior glass-forming ability through microalloying in cerium-based alloys, Phys. Rev. B 73 (2006) 092201.
[45] B. Zhang, D.Q. Zhao, M.X. Pan, W.H. Wang, A.L. Greer, Amorphous metallic plastic, Phys. Rev. Lett. 94 (2005) 205502.

View publication stats